

SDE-based Multiplicative Noise Removal

An Vuong, Thinh Nguyen

Oregon State University
vuonga2@oregonstate.edu, thinhq@oregonstate.edu

Abstract

Multiplicative noise, also known as speckle or pepper noise, commonly affects images produced by synthetic aperture radar (SAR), lasers, or optical lenses. Unlike additive noise, which typically arises from thermal processes or external factors, multiplicative noise is inherent to the system, originating from the fluctuation in diffuse reflections. These fluctuations result in multiple copies of the same signal with varying magnitudes being combined. Consequently, despeckling, or removing multiplicative noise, necessitates different techniques compared to those used for additive noise removal.

In this paper, we propose a novel approach using Stochastic Differential Equations based diffusion models to address multiplicative noise. We demonstrate that multiplicative noise can be effectively modeled as a Geometric Brownian Motion process in the logarithmic domain. Utilizing the Fokker-Planck equation, we derive the corresponding reverse process for image denoising. To validate our method, we conduct extensive experiments on two different datasets, comparing our approach to both classical signal processing techniques and contemporary CNN-based noise removal models. Our results indicate that the proposed method significantly outperforms existing methods on perception-based metrics such as FID and LPIPS, while maintaining competitive performance on traditional metrics like PSNR and SSIM. Code and appendix available at https://github.com/anvuongb/sde_multiplicative_noise_removal.

Introduction

Multiplicative noise removal is a long standing problem in computer vision and has been studied by many researchers over the past few decades (Huang, Ng, and Wen 2009)(Bioucas-Dias and Figueiredo 2010)(Huang et al. 2012)(Shan, Sun, and Guo 2019)(Feng and Zhu 2021). Unlike additive noise, which is usually the result of thermal fluctuations during image acquisition or transmission, multiplicative noise happens when multiple copies of the signal with random scaling factors are added together. This often happens due to the internal physical construction of the image capturing devices, i.e. optical lenses, radar/laser imaging, ultrasound sensors, etc. Because of this, removing multiplicative noise, sometimes referred to as despeckling, often requires more sophisticated approaches compared to its

preprint. Under review

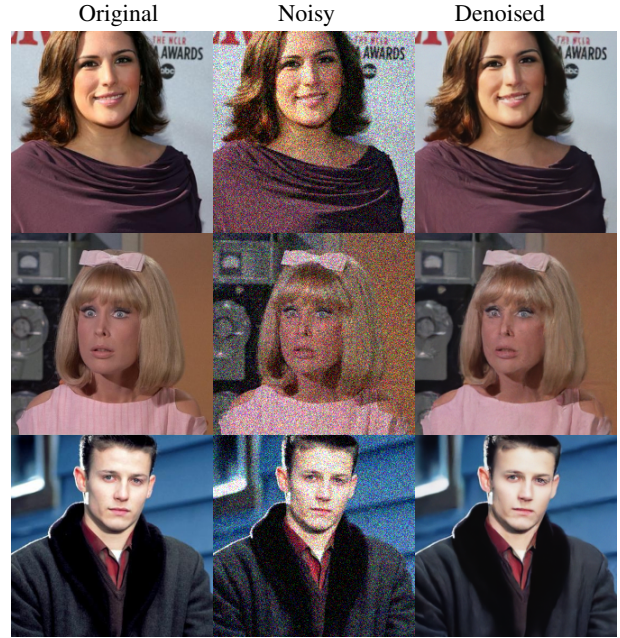


Figure 1: Samples generated by our methods, on images randomly selected from CelebA dataset. From left to right are the original, corrupted by multiplicative noise (noise level 0.08), and denoised versions.

counterpart additive noise. Popular approaches include modelling the noise using Partial Differential Equations (PDEs) (Yu and Acton 2002) (Chen et al. 2012), converting into additive domain and optimize using Total Variation (TV) objective (Shi and Osher 2008), and applying MAP estimation (Aubert and Aujol 2008). Classical methods based on block-matching technique also works decently for this problem (Dabov et al. 2007). More recently, deep learning based methods have been introduced with great successes in denoising performance (Zhang et al. 2017)(Wang et al. 2022)(Chen et al. 2022). These methods usually use image-to-image translation architecture, where the neural networks directly predict the clean images, or the amount of noise generated by the stochastic process, without much assumption on the noise dynamics. Thus, many of these models can be applied to reverse different kinds of corruptions, including

multiplicative noise. However, these techniques mostly rely on "per-pixel" metrics such as MSE, PSNR, or SSIM, which has been observed to not correlate well with human perception (Blau and Michaeli 2018).

In this work, we propose the novel application of Stochastic Differential Equations (SDEs) to perform multiplicative noise removal. We show that the dynamics of multiplicative noise is well captured by SDEs, specifically Geometric Brownian motion. We then derive the reverse SDEs which are used to generate denoised samples. By running extensive experiments on two different datasets, we demonstrate the effectiveness of our method on creating clean images that achieve high perception scores. We detail the construction of our approach in the next section.

Methodology

SDE and Diffusion models

In this section, we give a brief overview of Stochastic Differential Equations, Itô's calculus, and the application to generative modelling.

Let $\beta(t)$ be a Brownian motion indexed by time t , i.e. $\beta(t)$ is a random process with independent and zero-mean Gaussian increment, then the classic result from Itô's calculus gives

$$\int \beta(t)d\beta(t) = \frac{1}{2}\beta^2(t) - \frac{1}{2}t \quad (1)$$

or in a more compact differential form

$$\frac{1}{2}d\beta^2(t) = \beta(t)d\beta(t) + \frac{1}{2}dt \quad (2)$$

This seminal result plays a central role in solving SDE, whose informal definition can be given by the following differential equation

$$dx(t) = f(x(t), t)dt + L(x(t), t)d\beta(t) \quad (3)$$

where $f(\cdot)$, $L(\cdot)$ are some functions, $x(t)$ is the random process of interest, and $dx(t)$ represents the (random) infinitesimal change of $x(t)$. The remarkable thing about (3) is that, under some smoothness assumptions of $f(\cdot)$ and $L(\cdot)$, there exists a unique SDE that models the reverse process (Øksendal and Øksendal 2003):

$$\begin{aligned} dx(T-t) = & -f(x(T-t), T-t)dt \\ & + L(x(T-t), T-t)d\beta(T-t) \\ & + L^2(T-t)\nabla \log p_{T-t}dt \end{aligned} \quad (4)$$

where p_{T-t} denotes the distribution of $x(T-t)$. This result comes directly from the application of the Fokker-Planck equation, and is sometimes referred to as Anderson's theorem. The extension of these results to multivariate process is straightforward, and detailed proofs can be found in (Ito et al. 1951)(Øksendal and Øksendal 2003)(Särkkä and Solin 2019).

A crucial observation is that, if $\nabla \log p_{T-t}$ is known, then one can run equation (4) to generate new sample $x(T-t)$ that comes from data distribution $p_{T-t}(x)$. This motivates the search for an efficient method to estimate $\nabla \log p_{T-t}$, also known as the score function. Let us

now denote the estimation of $\nabla \log p(x)$ as $s_\theta(x)$, some function parameterized by θ , then the surprising result from (Hyvärinen and Dayan 2005) gives

$$\begin{aligned} \mathbb{E}_x \left[\frac{1}{2} \|\nabla \log p(x) - s_\theta(x)\|_2^2 \right] \\ \propto \mathbb{E}_x \left[\frac{1}{2} \|s_\theta(x)\|_2^2 + \text{trace}(\nabla s_\theta(x)) \right] \end{aligned} \quad (5)$$

From (5), one can parameterize $s_\theta(x)$ as a neural network and directly optimize using samples of x without needing the knowledge of $\nabla \log p(x)$. This result, along with Langevin sampling, was used in (Song and Ermon 2019) to train neural networks for images generation tasks that achieve high-quality results. In the follow-up papers (Song, Meng, and Ermon 2020)(Song and Ermon 2019), the authors tweaked the learning procedure to learn $\nabla \log p_{T-t}(x)$, instead of $\nabla \log p(x)$, this proved to be more stable and easier to implement, while achieving better results at the same time. In these works, the sampling was done using (4), instead of Langevin dynamics. This approach is referred to as Score-based Generative Models (SGMs).

In a parallel development, (Ho, Jain, and Abbeel 2020) proposed a similar framework from Markov chain perspective, which is named Diffusion Denoising Probabilistic Models (DDPM). DDPM formulation leads to a much simpler objective function, which is shown to be equivalent to (5) under Gaussian noise assumption (Vincent 2011). In this paper, we use the SDE-based formulation since it is more flexible, allowing us to directly model the desired underlying dynamics of the noise process.

Noise models

In this section, we introduce multiplicative noise, and show how SDE can be used to model the dynamics of this process.

A real-valued signal $x \in \mathbb{R}$ is corrupted by multiplicative noise is modeled as

$$\tilde{x} = \epsilon x \quad (6)$$

where $\epsilon \in \mathbb{R}$ is a random variable, usually modeled as having Gamma or Log-normal distribution, and \tilde{x} is the corrupted version of x . Here, we extend this noise process to multi-dimensional $\mathbf{x} \in \mathbb{R}^d$, with the assumption that this corruption affects each component independently

$$\tilde{\mathbf{x}} = \mathbf{x} \odot \epsilon \quad (7)$$

where $\epsilon \in \mathbb{R}^d$ and \odot represents the element-wise multiplication. We now show that (7) can be well modelled by the following SDE

$$d\mathbf{x} = \alpha(t)\mathbf{x}(t) \odot d\beta(t) \quad (8)$$

where $\alpha(t)$ is some time-varying scalar function and $\beta(t)$ is a Brownian motion on \mathbb{R}^d . Indeed, the solution to (8) (details

in the Appendix¹) is given as

$$x_{t,i} = x_{0,i} \exp \left(\int_0^t \frac{1}{2} \alpha^2(\tau) d\tau + \int_0^t \alpha(\tau) d\beta(\tau) \right) \quad (9)$$

$$= x_{0,i} \exp \left(- \int_0^t \frac{1}{2} \alpha^2(\tau) d\tau + \left(\int_0^t \alpha^2(\tau) d\tau \right)^{\frac{1}{2}} n \right) \quad (10)$$

$$n \sim \mathcal{N}(0, 1)$$

where $x_{t,i}$ denotes the i -th entry of $\mathbf{x}(t)$. Since n is Gaussian, the exponential term in (8) will follow Log-normal distribution, satisfying our previous assumption on ϵ . If we select $\mathbf{x}(0)$ to be the clean image \mathbf{x} , then with appropriate value of t , $\tilde{\mathbf{x}}$ can be well modelled by (8).

We can now apply Anderson’s theorem to derive the reverse SDE for (8) and use score-matching method from (Song et al. 2020) to construct a denoising model. But this formulation gives a rather complicated reverse SDE, as shown in the Appendix. For this reason, we propose to apply a simple logarithmic transformation to \mathbf{x} , this yields a much simpler reverse SDE, with the additional advantage of being able to apply the results from (Vincent 2011), making the loss function easier to derive.

Loss function in the logarithmic domain

Let us denote $y_{t,i} = \log x_{t,i}$. Now, equation (9) becomes

$$y_{t,i} = y_{0,i} - \int_0^t \frac{1}{2} \alpha^2(\tau) d\tau + \int_0^t \alpha(\tau) d\beta(\tau) \quad (11)$$

which can also be expressed in differential form to obtain the SDE

$$dy_{t,i} = -\frac{1}{2} \alpha^2(t) dt + \alpha(t) d\beta(t) \quad (12)$$

Equation (12) can also be written in vector form

$$d\mathbf{y}_t = -\frac{1}{2} \alpha^2(t) \mathbf{1} dt + \alpha(t) d\boldsymbol{\beta}(t) \quad (13)$$

which has the corresponding reverse SDE (proof in the Appendix)

$$d\mathbf{y}_{T-t} = \left(\frac{1}{2} \alpha^2(T-t) \mathbf{1} + \alpha^2(T-t) \nabla \log p_{T-t}(\mathbf{y}_{T-t}) \right) dt + \alpha(T-t) d\boldsymbol{\beta}(T-t) \quad (14)$$

where T is the terminal time index, i.e. at which the forward SDE (13) stopped.

Applying Euler-Maruyama discretization to (13) and (14), where $\alpha(t)$ is selected to be $\sqrt{\frac{d\sigma(t)}{dt}}$ with $\sigma(t)$ is some differentiable function having non-negative slope, gives the fol-

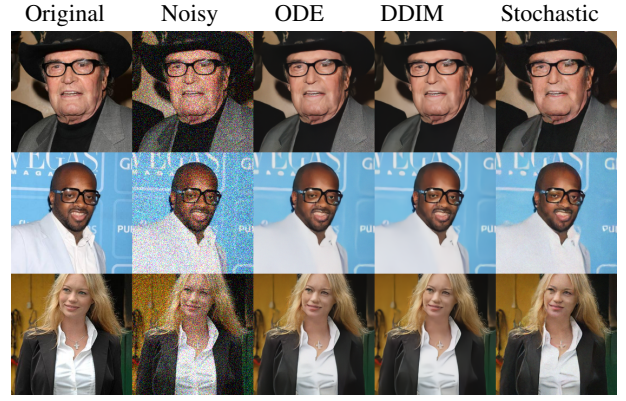


Figure 2: Comparing between different sampling techniques on randomly selected CelebA images, at noise level 0.12. The first two columns include the original images and their noised versions, respectively. These are followed by the results generated by our model using ODE, DDIM, and stochastic samplers, respectively. Full resolution version is available in supplemental materials.

lowing pair of SDEs

$$\begin{aligned} \mathbf{y}_k &= \mathbf{y}_{k-1} - \frac{1}{2} (\sigma(k) - \sigma(k-1)) \mathbf{1} \\ &\quad + \sqrt{\sigma(k) - \sigma(k-1)} \mathbf{n}_k \\ &= \mathbf{y}_0 - \frac{1}{2} (\sigma(k) - \sigma(0)) \mathbf{1} + \sqrt{\sigma(k) - \sigma(0)} \mathbf{n}_k \end{aligned} \quad (15)$$

$$\begin{aligned} \mathbf{y}_{K-k} &= \mathbf{y}_{K-k+1} \\ &\quad + \frac{1}{2} (\sigma(K-k+1) - \sigma(K-k)) (\mathbf{1} + \\ &\quad \quad 2\nabla \log p_{K-k+1}(\mathbf{y}_{K-k+1})) \\ &\quad + \sqrt{\sigma(K-k+1) - \sigma(K-k)} \mathbf{n}_k \\ \mathbf{n}_k &\sim \mathcal{N}(\mathbf{0}, \mathbf{1}) \end{aligned} \quad (16)$$

To derive the loss function, note that equation (15) has a Gaussian transition kernel $p(\mathbf{y}_k | \mathbf{y}_{k-1}) = \mathcal{N}(\mathbf{y}_k; \mathbf{y}_{k-1} - \frac{1}{2} (\sigma(k) - \sigma(k-1)) \mathbf{1}, \sigma(k) - \sigma(k-1))$. Thus, results from (Vincent 2011) applies, which states the following connection between SGMs and DDPMs: let $\mathbf{s}^*(\mathbf{x}_t, t)$ and $\mathbf{n}^*(\mathbf{x}_t, t)$ be the minimizers of SGM and DDPM objectives, respectively, then $\mathbf{n}^*(\mathbf{x}_t, t) = -\sqrt{\text{var}(\mathbf{x}_t)} \mathbf{s}^*(\mathbf{x}_t, t)$ if $p(\mathbf{x}_t | \mathbf{x}_{t-1})$ is Gaussian, where $\text{var}(\mathbf{x}_t)$ denotes the variance of the stochastic process at time t . This means the denoising objective from DDPM can be readily applied to our formulation in the logarithmic domain, giving the following trainable loss

$$\mathcal{L}_{\theta, \text{discete}} = \mathbb{E}_{\mathbf{y}} \mathbb{E}_k \left[\|\mathbf{n}_k + \sqrt{\sigma(k) - \sigma(0)} \mathbf{s}_{\theta}(\mathbf{y}_k, k)\|_2^2 \right] \quad (17)$$

where the plus sign is due to the score function being opposite in direction to the noise vector. Thus, by transforming the data into the logarithmic domain, we can take advantage

¹Technical Appendix is provided in Supplemental materials

of the simplicity of DDPM framework, while still being able to accurately capture our noise model thanks to the flexibility of SDE. Furthermore, since log is a bijective transformation for positive variables, we can easily recover our images from the samples generated in logarithmic domain by taking the exponential. The training and sampling procedures are summarized in Algorithms 1 and 2.

Algorithm 1: Training procedure of $\mathbf{s}_\theta(\mathbf{y}_k, k)$

Input Training data $\mathbf{x} \in \mathcal{X}$, noise schedule $\sigma(t)$, number of epochs E , total steps K

Output Score network $\mathbf{s}_\theta(\mathbf{y}_k, k)$, where $\mathbf{y} = \log \mathbf{x}$

```

1:  $i = 1$ 
2: while  $i \leq E$  do
3:   for  $\mathbf{x} \in \mathcal{X}$  do
4:      $\mathbf{y} = \log \mathbf{x}$ 
5:     Draw  $k \sim \mathcal{U}(0, K)$ 
6:     Calculate  $\mathbf{y}_k$  according to (15)
7:     Take gradient step on:
            $\mathbb{E}_{\mathbf{y}} \mathbb{E}_k \left[ \|\mathbf{n}_k + \sqrt{\sigma(k) - \sigma(0)} \mathbf{s}_\theta(\mathbf{y}_k, k)\|_2^2 \right]$ 
8:   end for
9:    $i = i + 1$ 
10: end while
11: Return  $\mathbf{s}_\theta(\mathbf{y}_k, k)$ 

```

Algorithm 2: Noise removal procedure (stochastic)

Input Corrupted image $\tilde{\mathbf{x}}$, number of denoising steps K

Output Denoised image $\hat{\mathbf{x}}$

```

1:  $k = 1, \mathbf{y}_K = \log \tilde{\mathbf{x}}$ 
2: while  $k \leq K$  do
3:    $\nabla \log p_{K-k+1} = \mathbf{s}_\theta(\mathbf{y}_{K-k+1}, K - k + 1)$ 
4:   Sample  $\mathbf{y}_{K-k}$  using (16)
5: end while
6: Return denoised image  $\hat{\mathbf{x}} = \exp(\mathbf{y}_0)$ 

```

Enhancing image quality by deterministic sampling

Since the sampling equation (14) is a stochastic process, given a noisy input, different runs will result in different denoised images, albeit with the same statistics. This might not be desirable in applications where determinism is required. Thus, we now give two deterministic sampling equations specifically for our proposed SDE. Experimentally, we show that samples generated deterministically achieve substantially better Fréchet inception distance (FID) (Heusel et al. 2017) and Learned Perceptual Image Patch Similarity (LPIPS) (Zhang et al. 2018) metrics

Probability flows. Following the idea in (Song et al. 2020), from (14), it can be shown that there exists an ODE counterpart whose marginals match that of (14), this ODE is given as

$$d\mathbf{y}_{T-t} = \left(\frac{1}{2} \alpha^2 (T-t) \mathbf{1} + \frac{1}{2} \alpha^2 (T-t) \nabla \log p_{T-t}(\mathbf{y}_{T-t}) \right) dt \quad (18)$$

which yields the discrete-time equation

$$\begin{aligned} \mathbf{y}_{K-k} &= \mathbf{y}_{K-k+1} \\ &+ \frac{1}{2} \left(\sigma(K-k+1) - \sigma(K-k) \right) \left(\mathbf{1} + \nabla \log p_{K-k+1}(\mathbf{y}_{K-k+1}) \right) \end{aligned} \quad (19)$$

Implicit probabilistic models. From the works of (Mohamed and Lakshminarayanan 2016) (Song, Meng, and Ermon 2020), given a stochastic process with Markov transition kernel $p(\mathbf{z}_{t-1}|\mathbf{z}_t)$, one can design another process with non-Markov transition kernel $q(\mathbf{z}_{t-1}|\mathbf{z}_t, \mathbf{z}_0)$ whose marginals match, i.e $q(\mathbf{z}_{t-1}|\mathbf{z}_t) = p(\mathbf{z}_{t-1}|\mathbf{z}_t)$. For our discretized SDE in (15), its non-Markov counterpart is given as (derivations can be found in Appendix)

$$q(\mathbf{y}_{k-1}|\mathbf{y}_k, \mathbf{y}_0) = \mathcal{N}(\boldsymbol{\mu}_k, \boldsymbol{\Sigma}_k) \quad (20)$$

$$\begin{aligned} \boldsymbol{\mu}_k &= \mathbf{y}_0 - \frac{1}{2} \eta(k-1) \mathbf{1} \\ &+ \frac{\sqrt{\eta(k-1) - \zeta_k^2}}{\sqrt{\eta(k)}} (\mathbf{y}_k - \mathbf{y}_0 + \frac{1}{2} \eta(k) \mathbf{1}) \end{aligned} \quad (21)$$

$$\boldsymbol{\Sigma}_k = \zeta_k^2 \mathbf{I} \quad (22)$$

where ζ_k^2 is a new parameter controlling the variance of the process, and $\eta(k) = \sigma(k) - \sigma(0)$. For deterministic sampling, we can set $\zeta_k^2 = 0$ and obtain the sampling equations

$$\begin{aligned} \mathbf{y}_{k-1} &= \hat{\mathbf{y}}_0 - \frac{1}{2} \eta(k-1) \mathbf{1} \\ &+ \frac{\sqrt{\eta(k-1)}}{\sqrt{\eta(k)}} (\mathbf{y}_k - \hat{\mathbf{y}}_0 + \frac{1}{2} \eta(k) \mathbf{1}) \end{aligned} \quad (23)$$

and $\hat{\mathbf{y}}_0$ is given as

$$\hat{\mathbf{y}}_0 = \mathbf{y}_k + \frac{1}{2} \eta(k) \mathbf{1} + \eta(k) \mathbf{s}_\theta(\mathbf{y}_k, k) \quad (24)$$

where $\mathbf{s}_\theta(\mathbf{y}_k, k)$ is the output of the neural network defined by the objective (17). Equation (24) can be thought of as the best possible prediction of \mathbf{y}_0 in single-step using \mathbf{y}_k . We note that this approach defines an implicit model that matches the marginals of (15), so the trained $\mathbf{s}_\theta(\mathbf{y}_k, k)$ can be reused even though we make no use of the original SDE during sampling. This sampler is referred to as Denoising Diffusion Implicit Models (DDIMs) in the literature.

Sampling procedure for these two techniques are provided in Algorithm 3 and 4.

Experiments

Experiment settings

We ran our experiments on CelebA (Liu et al. 2015) and UC Merced Land Use (Yang and Newsam 2010) datasets, using U-Net (Ronneberger, Fischer, and Brox 2015) as the backbone architecture for our neural networks. The training was done on 100,000 images from the CelebA dataset, while testing was performed on 2,096 images from CelebA holdout set and another 2,096 images from UC Merced Land Use, images were resized to 224x224 pixels. We did not finetune

Sampling technique	FID ↓	LPIPS ↓	PSNR ↑	SSIM ↑
ODE	13.9156	0.0365	31.8902	0.9348
DDIM	25.3188	0.0882	28.6549	0.9032
Stochastic	32.3811	0.1075	26.8267	0.8493

Table 1: Comparison of different sampling techniques on CelebA dataset at noise level 0.12

Noise level	Model	FID ↓	LPIPS ↓	PSNR ↑	SSIM ↑
0.04	Ours (ODE)	13.9156	0.0365	31.8902	0.9348
	NAFNet	20.5896	0.0503	34.0764	0.9661
	DnCNN	26.8650	0.0726	33.1393	0.9542
	SRAD	47.7516	0.2374	27.5801	0.8476
	CBM3D	25.1978	0.1282	29.5931	0.9067
0.08	Ours (ODE)	19.0333	0.0580	29.8902	0.9148
	NAFNet	25.3441	0.0693	32.4876	0.9546
	DnCNN	27.7345	0.0834	31.5783	0.9426
	SRAD	60.6093	0.3162	25.7904	0.7835
	CBM3D	31.2749	0.1774	27.4770	0.8726
0.12	Ours (ODE)	24.3077	0.0774	28.5567	0.8994
	NAFNet	27.0304	0.0805	31.5588	0.9466
	DnCNN	33.2722	0.1113	30.5007	0.9281
	SRAD	70.4303	0.3853	24.3354	0.7311
	CBM3D	36.2575	0.2128	26.1749	0.8481

Table 2: Comparison of different denoising methods for various metrics at different noise levels on CelebA dataset. The best performance for each metric is highlighted in bold.

Algorithm 3: Noise removal procedure (ODE)

Input Corrupted image $\tilde{\mathbf{x}}$, number of denoising steps K

Output Denoised image $\hat{\mathbf{x}}$

- 1: $k = 1, \mathbf{y}_K = \log \tilde{\mathbf{x}}$
 - 2: **while** $k \leq K$ **do**
 - 3: $\nabla \log p_{K-k+1} = \mathbf{s}_\theta(\mathbf{y}_{K-k+1}, K - k + 1)$
 - 4: Compute \mathbf{y}_{K-k} using (19)
 - 5: $k = k + 1$
 - 6: **end while**
 - 7: Return denoised image $\hat{\mathbf{x}} = \exp(\mathbf{y}_0)$
-

Algorithm 4: Noise removal procedure (DDIM)

Input Corrupted image $\tilde{\mathbf{x}}$, number of denoising steps K

Output Denoised image $\hat{\mathbf{x}}$

- 1: $k = K, \mathbf{y}_K = \log \tilde{\mathbf{x}}$
 - 2: **while** $k \leq K$ **do**
 - 3: Calculate
 - 4: $\nabla \log p_k = \mathbf{s}_\theta(\mathbf{y}_k, k)$
 - 5: Compute $\hat{\mathbf{y}}_0$ using (24)
 - 6: Compute \mathbf{y}_{k-1} using (23)
 - 7: $k = k - 1$
 - 8: **end while**
 - 9: Return denoised image $\hat{\mathbf{x}} = \exp(\mathbf{y}_0)$
-

on the land use dataset since we wanted to test the generalization of directly modeling the noise dynamics.

For baseline models, we have selected several denoising methods, ranging from classical signal processing techniques to modern CNN-based frameworks:

- The block-matching and 3D filtering (BM3D) was proposed in (Dabov et al. 2007), it partitions the image into multiple smaller patches and performs collaborative filtering to remove the noise. The method takes advantage of redundancy and consistent information across patches to generate a clean image, it achieved state-of-the-art performance at the times without requiring prior knowledge about noise statistics.
- Speckle reducing anisotropic diffusion (SRAD), proposed in (Yu and Acton 2002), is a method specifically designed for despeckling or multiplicative noise removal. It assumes a set of partial differential equations modeling the noise characteristics and iteratively adjusts the value of each pixel based on the local intensity variations.
- In (Zhang et al. 2017), DnCNN was proposed to perform Gaussian denoising in latent space using CNN and residual learning. It popularized the idea of learning the noise (residuals) of a noisy image instead of directly learning the clean version. DnCNN remains an important tool today and is widely available in image processing toolboxes such as Matlab.
- NAFNet (Chen et al. 2022), the current state-of-the-art in noise removal and image restoration. It incorporates multiple advances made by DnCNN, HINet (Chen et al. 2021), SwinIR (Liang et al. 2021), BasicSR (Wang et al.

2022) and others. We make comparison with the width-64 version of NAFNet, since this model has 116M parameters, which is comparable to ours, which has 108M.

Regarding training settings, we trained our model with $T = 500$ diffusion steps, linear noise schedule $\sigma(k) \in [0.0001, 0.02]$, and Adam optimizer (Kingma 2014). For DnCNN² and NAFNet³, we followed the optimal training options recommended by the authors on Github. All models are trained for 100 epochs. Training was done on 2x RTX3090 under Ubuntu using Pytorch framework. Since DnCNN and NAFNet need to be trained for some specific noise levels, we chose three noise variance levels $[0.04, 0.08, 0.12]$ for the noise term in (9), this corresponds to $T = 100, 200, 300$ in our diffusion process formulation. We note that, while DnCNN and NAFNet need to be trained for each noise level, our framework only needs to be trained once, then inference can be run at different noise levels since the noise dynamics is already captured by the SDE formulation.

For evaluation metrics, we chose to evaluate on perception-based metrics FID, LPIPS and traditional signal processing metrics PSNR, SSIM. While PSNR and SSIM are important measurements in computer vision, they have been shown to not correlate well with human perception on image restoration tasks (Zhang et al. 2018). In our experiments, we also observed substantial discrepancies between these two types of metrics, more detailed discussion is provided in the next section.

Our code is provided in the supplemental materials.

Experiment results

Sampling techniques. We evaluate our model with three different sampling techniques: stochastic sampling (16), ODE sampling (19), and DDIM sampling (23), on images from CelebA holdout set, generated from noise level 0.12. Results are presented in Table 1. It can be seen that samples generated using ODE technique perform substantially better across all metrics, especially in FID and LPIPS. Compared to stochastic sampling, deterministic samplers are up to 57% better at FID, and 66% better at LPIPS. This results in observable differences in generated samples, as can be seen from the qualitative examples provided in Figure 2.

Results on CelebA dataset. Quantitative results are presented in Table 2. Compared to the state-of-the-art model NAFNet, our method shows slightly worse performance in "per-pixel" metrics, while achieving significantly better FID and LPIPS scores, across all tested noise levels. This is also true when comparing to DnCNN. We note that DnCNN and NAFNet were architected to directly optimize PSNR during training, thus these models strive to achieve the best fidelity at the cost of diverging from the input distribution. For classical methods, CBM3D (the RGB version of BM3D) performs respectably, sometimes even coming close to DnCNN. In contrast, SRAD falls far behind in all metrics, we suspect this is because the tests were conducted

²<https://github.com/cszn/DnCNN>

³<https://github.com/megvii-research/NAFNet>

Original Noisy Ours NAFNet DnCNN SRAD BM3D



Figure 3: Comparing between different denoising models on randomly selected CelebA images, at noise level 0.08. The first two columns include the original images and their noised versions, respectively. These are followed by the results generated by our method and other popular techniques. Full resolution version is available in supplemental materials.

Original Noisy Ours NAFNet DnCNN SRAD BM3D

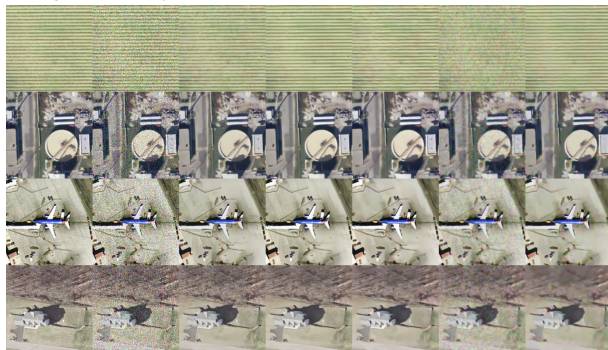


Figure 4: Comparing between different denoising models on randomly selected UC Merced Land Use images, at noise level 0.12. The first two columns include the original images and their noised versions, respectively. These are followed by the results generated by our method and other popular techniques. Full resolution version is available in supplemental materials.

using RGB images, and SRAD was originally designed for grayscale samples only.

These observations can also be seen in Figure 3, where we present denoising results of these models at noise level 0.08. Compared to our method, other techniques suffer from over-smoothing and they usually generate samples that lack high-frequency details. This is the drawback of using PSNR as an optimization objective, where the denoisers have the tendency of collapsing into the mean statistics of the images, creating smoothing effect. In contrast, our proposed model tends to be much better at preserving finer details, such as facial hair and clothes wrinkles.

Out-of-distribution results on Land Use dataset. To evaluate the generalization capability of our method, we re-run the previous experiments on the UC Merced Land Use dataset, which is a small dataset (containing 2,096 samples) captured from satellites. Besides being out-of-distribution,

Noise level	Model	FID ↓	LPIPS ↓	PSNR ↑	SSIM ↑
0.04	Ours (ODE)	35.7451	0.0753	31.2300	0.9137
	NAFNet	51.4628	0.1063	32.4929	0.9322
	DnCNN	111.3414	0.1628	31.8040	0.9217
	SRAD	70.5202	0.3565	27.7434	0.8318
	CBM3D	74.0214	0.2553	29.8244	0.8836
0.08	Ours (ODE)	50.6311	0.1067	29.6971	0.8887
	NAFNet	71.6357	0.1403	30.9993	0.9131
	DnCNN	126.2552	0.1867	30.2481	0.8978
	SRAD	91.9534	0.4235	26.3913	0.7772
	CBM3D	89.7331	0.3181	28.1350	0.8433
0.12	Ours (ODE)	63.2679	0.1333	28.8183	0.8727
	NAFNet	77.2864	0.1644	30.0889	0.8977
	DnCNN	138.2030	0.2361	29.2134	0.8710
	SRAD	107.6315	0.4712	25.2329	0.7247
	CBM3D	100.1406	0.3570	27.1042	0.8144

Table 3: Comparison of different denoising methods for various metrics at different noise levels on UC Merced Land Use dataset. The best performance for each metric is highlighted in bold.

we note that this is a much harder dataset to do denoising on, due to the blurriness and color shifting of satellite imaging. We present quantitative results in Table 3. While there is large degradation in performance across the board, we again see that our method achieves the best FID and LPIPS scores, while being slightly worse in terms of PSNR and SSIM. Surprisingly, DnCNN performs much worse in terms of FID, while remaining competitive in the other metrics. This could be related to the incorrect assumption of the FID calculation, which was recently discussed in (Jayasumana et al. 2024).

Qualitatively, from Figure 4, it is observed that our method retains finer details of the images, especially in the first and the last examples. NAFNet and DnCNN produce over-smoothed samples, losing details of the ground, while SRAD and BM3D generate images that completely lack high-frequency components.

Overall, we see that our method achieves competitive performance on PSNR and SSIM, while producing more realistic samples that are closer to the true input distribution, as measured by FID and LPIPS metrics. Furthermore, we show empirically that the method can generalize well to out-of-distribution dataset, which could be crucial in applications where data samples are limited. We provide more qualitative examples in the Appendix.

Related works

Over the last few years, with the advances of deep learning, there has been active research in applying CNN to image denoising problems, especially for speckle or multiplicative noise. Notable works can be found in (Li et al. 2021)(Choi and Jeong 2018)(Feng et al. 2020). In these texts, the common theme is to perform image-to-image translation with a Convolutional neural network (CNN) acting as the mapping function. This CNN is usually trained to minimize MSE or PSNR loss directly on the pairs of clean and noisy images. Some works propose to use specially-crafted features as the input, such as frequency features (Yang et al.

2022), or wavelet features (Zhang, Li, and Li 2019), and sub-bands (Liu et al. 2021). These works are usually limited to grayscale images, and are often matched in performance by DnCNN, and can be beaten by NAFNet.

Recently, there is a line of works applying diffusion technique to this problem. In (Guha and Acton 2023), the authors propose a DDPM-like architecture for despeckling, but this model needs to be re-trained for each noise level. Similarly, (Perera et al. 2023)(Xiao, Huang, and Zhang 2023) also use DDPM framework with minor modifications. These works still limit their testing to greyscale images only. We find the discussion in (Pearl et al. 2023) to be the most related to our work, albeit with different assumption of the noise characteristics and the construction of the diffusion process, where the authors still rely on the DDPM equations.

To the best of our knowledge, we are the first to directly model this problem using SDE, which captures the dynamics of the noise process, and derive the sampling equation which is then used to perform denoising.

Conclusion

In conclusion, this paper introduces a novel SDE-based diffusion model for removing multiplicative noise. The work presents the construction of the forward and reverse SDEs that directly captures the dynamics of the noise model. In addition, it also establishes the training objective as well as multiple different sampling equations based on Probability flows and DDIM techniques. The proposed model is compared to classical image processing algorithms, including BM3D and SRAD, as well as the modern CNN-based methods. Extensive experiments on different datasets demonstrate that our method outperforms the current state-of-the-art denoising models in perception-based metrics across all noise levels, while still remaining competitive in PSNR and SSIM.

Going forward, we will explore the application of diffusion steps reduction techniques to noise removal problems.

While these techniques have been applied successfully in many generative tasks, we find that it greatly reduces the quality of generated samples in our problem. Thus, care need to be taken when dealing with tasks that are sensitive to small perturbation like denoising. Furthermore, while deterministic sampling is usually used to speedup generation, it is a desirable property in noise removal tasks. Specifically, we would like the process to produce the exact clean image, not something close in terms of distribution, which is modelled by the current diffusion loss. This has connections to conditioning using Doob's h -transform, and could hold interesting research venue, we leave it to future explorations.

Reproducibility Checklist

Please refer to the Technical Appendix.

References

- Aubert, G.; and Aujol, J.-F. 2008. A variational approach to removing multiplicative noise. *SIAM journal on applied mathematics*, 68(4): 925–946.
- Bioucas-Dias, J. M.; and Figueiredo, M. A. 2010. Multiplicative noise removal using variable splitting and constrained optimization. *IEEE Transactions on Image Processing*, 19(7): 1720–1730.
- Blau, Y.; and Michaeli, T. 2018. The perception-distortion tradeoff. In *Proceedings of the IEEE conference on computer vision and pattern recognition*, 6228–6237.
- Chen, B.; Cai, J.-L.; Chen, W.-S.; and Li, Y. 2012. A multiplicative noise removal approach based on partial differential equation model. *Mathematical Problems in Engineering*, 2012(1): 242043.
- Chen, L.; Chu, X.; Zhang, X.; and Sun, J. 2022. Simple Baselines for Image Restoration. *arXiv preprint arXiv:2204.04676*.
- Chen, L.; Lu, X.; Zhang, J.; Chu, X.; and Chen, C. 2021. HINet: Half Instance Normalization Network for Image Restoration. In *Proceedings of the IEEE/CVF Conference on Computer Vision and Pattern Recognition (CVPR) Workshops*, 182–192.
- Choi, H.; and Jeong, J. 2018. Speckle noise reduction in ultrasound images using SRAD and guided filter. In *2018 International Workshop on Advanced Image Technology (IWAIT)*, 1–4. IEEE.
- Dabov, K.; Foi, A.; Katkovnik, V.; and Egiazarian, K. 2007. Image denoising by sparse 3-D transform-domain collaborative filtering. *IEEE Transactions on image processing*, 16(8): 2080–2095.
- Feng, D.; Wu, W.; Li, H.; and Li, Q. 2020. Speckle noise removal in ultrasound images using a deep convolutional neural network and a specially designed loss function. In *Multiscale Multimodal Medical Imaging: First International Workshop, MMMI 2019, Held in Conjunction with MICCAI 2019, Shenzhen, China, October 13, 2019, Proceedings 1*, 85–92. Springer.
- Feng, X.; and Zhu, X. 2021. Models for multiplicative noise removal. *Handbook of Mathematical Models and Algorithms in Computer Vision and Imaging: Mathematical Imaging and Vision*, 1–34.
- Guha, S.; and Acton, S. T. 2023. Sddpm: Speckle denoising diffusion probabilistic models. *arXiv preprint arXiv:2311.10868*.
- Heusel, M.; Ramsauer, H.; Unterthiner, T.; Nessler, B.; and Hochreiter, S. 2017. Gans trained by a two time-scale update rule converge to a local nash equilibrium. *Advances in neural information processing systems*, 30.
- Ho, J.; Jain, A.; and Abbeel, P. 2020. Denoising diffusion probabilistic models. *Advances in neural information processing systems*, 33: 6840–6851.
- Huang, Y.-M.; Moisan, L.; Ng, M. K.; and Zeng, T. 2012. Multiplicative noise removal via a learned dictionary. *IEEE Transactions on Image Processing*, 21(11): 4534–4543.
- Huang, Y.-M.; Ng, M. K.; and Wen, Y.-W. 2009. A new total variation method for multiplicative noise removal. *SIAM Journal on imaging sciences*, 2(1): 20–40.
- Hyvärinen, A.; and Dayan, P. 2005. Estimation of non-normalized statistical models by score matching. *Journal of Machine Learning Research*, 6(4).
- Ito, K.; Itô, K.; Itô, K.; Mathématicien, J.; Itô, K.; and Mathématicien, J. 1951. *On stochastic differential equations*, volume 4. American Mathematical Society New York.
- Jayasumana, S.; Ramalingam, S.; Veit, A.; Glasner, D.; Chakrabarti, A.; and Kumar, S. 2024. Rethinking fid: Towards a better evaluation metric for image generation. In *Proceedings of the IEEE/CVF Conference on Computer Vision and Pattern Recognition*, 9307–9315.
- Kingma, D. 2014. Adam: a method for stochastic optimization. *arXiv preprint arXiv:1412.6980*.
- Li, D.; Yu, W.; Wang, K.; Jiang, D.; and Jin, Q. 2021. Speckle noise removal based on structural convolutional neural networks with feature fusion for medical image. *Signal Processing: Image Communication*, 99: 116500.
- Liang, J.; Cao, J.; Sun, G.; Zhang, K.; Van Gool, L.; and Timofte, R. 2021. SwinIR: Image Restoration Using Swin Transformer. *arXiv preprint arXiv:2108.10257*.
- Liu, G.; Kang, H.; Wang, Q.; Tian, Y.; and Wan, B. 2021. Contourlet-CNN for SAR image despeckling. *Remote Sensing*, 13(4): 764.
- Liu, Z.; Luo, P.; Wang, X.; and Tang, X. 2015. Deep Learning Face Attributes in the Wild. In *Proceedings of International Conference on Computer Vision (ICCV)*.
- Mohamed, S.; and Lakshminarayanan, B. 2016. Learning in implicit generative models. *arXiv preprint arXiv:1610.03483*.
- Øksendal, B.; and Øksendal, B. 2003. *Stochastic differential equations*. Springer.
- Pearl, N.; Brodsky, Y.; Berman, D.; Zomet, A.; Acha, A. R.; Cohen-Or, D.; and Lischinski, D. 2023. Svrn: Spatially-variant noise removal with denoising diffusion. *arXiv preprint arXiv:2306.16052*.

- Perera, M. V.; Nair, N. G.; Bandara, W. G. C.; and Patel, V. M. 2023. SAR despeckling using a denoising diffusion probabilistic model. *IEEE Geoscience and Remote Sensing Letters*, 20: 1–5.
- Ronneberger, O.; Fischer, P.; and Brox, T. 2015. U-net: Convolutional networks for biomedical image segmentation. In *Medical image computing and computer-assisted intervention—MICCAI 2015: 18th international conference, Munich, Germany, October 5-9, 2015, proceedings, part III 18*, 234–241. Springer.
- Särkkä, S.; and Solin, A. 2019. *Applied stochastic differential equations*, volume 10. Cambridge University Press.
- Shan, X.; Sun, J.; and Guo, Z. 2019. Multiplicative noise removal based on the smooth diffusion equation. *Journal of Mathematical Imaging and Vision*, 61: 763–779.
- Shi, J.; and Osher, S. 2008. A nonlinear inverse scale space method for a convex multiplicative noise model. *SIAM Journal on imaging sciences*, 1(3): 294–321.
- Song, J.; Meng, C.; and Ermon, S. 2020. Denoising diffusion implicit models. *arXiv preprint arXiv:2010.02502*.
- Song, Y.; and Ermon, S. 2019. Generative modeling by estimating gradients of the data distribution. *Advances in neural information processing systems*, 32.
- Song, Y.; Sohl-Dickstein, J.; Kingma, D. P.; Kumar, A.; Ermon, S.; and Poole, B. 2020. Score-based generative modeling through stochastic differential equations. *arXiv preprint arXiv:2011.13456*.
- Vincent, P. 2011. A connection between score matching and denoising autoencoders. *Neural computation*, 23(7): 1661–1674.
- Wang, X.; Xie, L.; Yu, K.; Chan, K. C.; Loy, C. C.; and Dong, C. 2022. BasicSR: Open Source Image and Video Restoration Toolbox. <https://github.com/XPixelGroup/BasicSR>.
- Xiao, S.; Huang, L.; and Zhang, S. 2023. Unsupervised sar despeckling based on diffusion model. In *IGARSS 2023-2023 IEEE International Geoscience and Remote Sensing Symposium*, 810–813. IEEE.
- Yang, T.; Wang, W.; Cheng, G.; Wei, M.; Xie, H.; and Wang, F. L. 2022. FDDL-Net: frequency domain decomposition learning for speckle reduction in ultrasound images. *Multimedia Tools and Applications*, 81(29): 42769–42781.
- Yang, Y.; and Newsam, S. 2010. Bag-of-visual-words and spatial extensions for land-use classification. In *Proceedings of the 18th SIGSPATIAL international conference on advances in geographic information systems*, 270–279.
- Yu, Y.; and Acton, S. T. 2002. Speckle reducing anisotropic diffusion. *IEEE Transactions on image processing*, 11(11): 1260–1270.
- Zhang, J.; Li, W.; and Li, Y. 2019. SAR image despeckling using multiconnection network incorporating wavelet features. *IEEE Geoscience and Remote Sensing Letters*, 17(8): 1363–1367.
- Zhang, K.; Zuo, W.; Chen, Y.; Meng, D.; and Zhang, L. 2017. Beyond a Gaussian Denoiser: Residual Learning of Deep CNN for Image Denoising. *IEEE Transactions on Image Processing*, 26(7): 3142–3155.
- Zhang, R.; Isola, P.; Efros, A. A.; Shechtman, E.; and Wang, O. 2018. The Unreasonable Effectiveness of Deep Features as a Perceptual Metric. In *CVPR*.